Frequency of persistent blocking and ridge events related to precipitation over eastern China during August and its preceding atmospheric signals

Bo Zhang[1], Ge Liu[2,3*], Yuejian Zhu[4], Ning Shi[3]

[1]*National Meteorological Center, China meteorological administration, Beijing, China*

[2]*State Key Laboratory of Severe Weather, Chinese Academy of Meteorological Sciences, Beijing, China*

[3]*Collaborative Innovation Centre on Forecast and Evaluation of Meteorological Disasters, Nanjing University of Information Science and Technology, Nanjing, China*

[4]*Environmental Modeling Center, NCEP/NOAA/NWS, Silver Spring, USA*

Submitted to Weather and Forecasting on March 6, 2019

*Corresponding author address: Dr. Ge Liu, State Key Laboratory of Severe Weather, Chinese Academy of Meteorological Sciences, 46 Zhong-Guan-Cun South Avenue, Beijing 100081, China.

E-mail: liuge@cma.gov.cn

Telephone: 86-10-68407867

ABSTRACT: Based on a new approach that can effectively recognize both persistent ridges and blockings (maxima) of 500-hPa geopotential height (500Z; PMZ) events, the contributions of the frequency of PMZ events (FOPE) over different regions of Eurasia to precipitation over eastern China are investigated. The results reveal that, relative to the FOPE over other ranges of longitude, that over 110°E–130°E, near the Stanovoy Mountains (SM) and Okhotsk Sea (OS) region, is most significantly correlated with precipitation over the middle and lower reaches of Yangtze River (MLRYR) during summer, particularly in August. Through southward Rossby-wave energy dispersion of the geopotential height anomaly near the OS, the 110°E–130°E FOPE is closely related to the high- and mid-latitude anomaly centers of East Asian/Pacific (EAP) pattern which, together with the low-latitude anomaly center of the EAP pattern, induce a convergence of cold and warm flows over the MLRYR, and hence modulate precipitation *in situ*. The synthesized effect of July geopotential height anomaly over the Balkhash Lake (BL) and that over the Caucasus region (CR), which is closely connected with a Silk Road Pattern, can stimulate and intensify a relay-like northeastward extension of geopotential height anomaly from the BL to OS regions during July–August. This northeastward extension implies that high-pressure systems appear over the BL during July and then gradually move northeastwards during July–August and finally facilitate the occurrence of 110°E–130°E PMZ events during August. As such, a July BL-CR height index measuring both the CR and BL height anomalies gives a good performance in predicting the August 110°E–130°E FOPE, which also facilitates, to some extent, the prediction of August MLRYR

precipitation.

KEY WORDS Blocking; ridge; summer precipitation; eastern China; prediction

1. Introduction

Blocking is one of the most important atmospheric circulation systems at the middle and high latitudes, contributing to weather and climate anomalies over different regions during different seasons. For example, anomalous evolution of blocking can trigger large-range cold waves during winter and spring (Lukas et al., 2017; Buehler et al., 2011; Pfahl and Wernli, 2012; Cattiaus et al., 2010; Ye et al., 2015). During summer, persistent blocking can induce local high pressure that prolongs dry and warm surface conditions, and therefore lead to severe droughts and heatwaves (Green, 1977; Dole et al., 2011; Matsueda, 2011; Hoskins and Woollings, 2015; Horton et al., 2016). Also, the maintenance of Eurasian blocking highs plays an important role in adjusting large-scale droughts and floods over different regions of China (Gu et al., 2016; Yu and Lin, 2006; Lu et al., 1999; Wu et al., 1994; Bi and Ding, 1992; Zhang and Tao, 1998).

Besides blockings, it is found that open ridges are able to cause high-impact weather and climate anomalies in certain cases, such as an extreme heatwave in early August 2003 over Europe (Black et al., 2004) and an extreme cold event in East Asia (Bueh and Xie, 2015). Actually, open ridge, omega-shape blocking, and closed blocking often constitute a life cycle of the development of high pressure anomaly, which consecutively affects synoptic-scale temperature and precipitation anomalies. When the processes frequently take place, they can even adjust climate anomalies on seasonal timescale. For instance, strong persistent high-pressure (anticyclone) anomaly over the Okhotsk Sea (OS) region can cause floods over the middle and lower reaches of Yangtze River (MLRYR) during summer (Zhang and Tao, 1998), in which the summer-mean high-pressure anomaly (anticyclone) should be considered as a common outcome of both blockings and open ridges. It is well known that the MLRYR is an important area bearing on the sustainable development in ecology and economy of China (Zhang et al., 2008). However, this area experienced frequent floods, which was the direct result of abnormally more precipitation that occurred during summer (Yi and Li, 2001). It is obviously important to investigate the relationship of summer precipitation over the MLRYR with blocking and open ridges and to further explore associated preceding signals.

The abovementioned studies showed the importance of blockings and open ridges in affecting temperature and precipitation anomalies on different timescales. However, the definitions of most blocking indices cannot effectively recognize ridges of different types, such as persistent ridges, immature blockings and omega-shape blockings. Recently, a Lagrangian objective approach, which is different from Eulerian objective method (Kaas and Branstator, 1993; Renwick, 2005; Parsons et al., 2016), is developed to identify and track persistent open ridges of 500-hPa geopotential height either as an individual event or as a part attached to a blocking anticyclone (Liu et al., 2017). This new approach successfully captures the formation and moving of open ridges and closed blockings, thus we use it to identify persistent open ridges and blocking highs (maxima) of 500-hPa geopotential height (Z500; PMZ) in the present study.

Based on the PMZ events identified by the new approach (Liu et al., 2017), the relationships between precipitation over eastern China and the frequency of PMZ events (FOPE) over different regions of Eurasia during summer are explored, which can disclose where the key region of PMZ events influencing precipitation over eastern China is. In addition, preceding atmospheric signal of the FOPE over the key region is investigated, which is, to some extent, favorable for understanding and improving the prediction of precipitation over eastern China.

The rest of this paper is organized as follows: The datasets and methods are described in section 2. The relationship between the FOPE and precipitation over eastern China during summer, as well as associated mechanism that explains this relationship, are presented in section 3. The preceding atmospheric signals of the FOPE are investigated in section 4. Finally, a summary and a discussion are provided in section 5.

2. Data and methods

2.1 Data

The daily 500-hPa geopotential height with the spatial resolution of 2.5° by 2.5°, which is obtained from the National Centers for Environmental Prediction (NCEP) and National Center for Atmospheric Research (NCAR) reanalysis dataset (Kalnay et al., 1996), is applied in identifying the PMZ events. The NCEP monthly mean pressure-level geopotential height and ***u***- and ***v***-wind (Kalnay et al., 1996) and the monthly values of the Climate Prediction Center Merged Analysis of Precipitation (CMAP) with the spatial resolution of 2.5° by 2.5° (Xie and Arkin, 1997) are also utilized in this study. The above datasets are extracted for the period 1979 to 2017.

2.2 Methods

Following Liu et al (2017), a PMZ event can be identified when its core includes a local maximum of eddy anomaly (Z*) of Z500 and its neighboring grid points whose values are greater than 100 GPMs and decrease radially to about 20 GPMs smaller than the maximum value. In addition, if two cores share at least on grid point and move no greater than 10° longitude per day on consecutive Z* maps, they belong to one PMZ event. The PMZ event should persist for 2 days or longer; otherwise it cannot be regarded as a PMZ event. To exclude weak ridges, each of the tracked cores is expanded to contain more contiguous points whose Z* value decrease radially to about 100 GPMs.

The FOPE is defined as follows. If a PMZ event appears (including occurs and passes through) over a grid point in a day, one time is counted in this grid point. If a persistent PMZ event occupies a grid point for *n* days, *n* times are counted in this grid point. The FOPE over a region is calculated by the averaged times in each grid point within this region, which can therefore reflect the length of time when PMZ events govern this region.

Correlation and regression are also used in the present study to examine the relationships between variables. Since the variation of one variable may sometimes be caused by multiple factors, a linear fitting method is applied to reveal the independent effect of one factor after removing the variation of the other factor (Hu et al., 2012). In this study, unless otherwise stated, the Student's t-test is employed to evaluate the statistical significance of correlation and regression analyses.

3. Relationship between the FOPE and precipitation over eastern China

3.1 Climate distribution of the FOPE and precipitation

Before exploring the relationship between the FOPE and precipitation over eastern China during summer, we first detect the climate mean distributions of FOPE for four seasons (spring, summer, autumn, and winter) during the period 1979–2017, which are shown in Figure 1. During summer the area with the FOPE higher than 5 extends eastwards from Europe to eastern Russia, around the longitude of 145°E, to the north of the OS (Figure 1b), while the area with the FOPE higher than 5 can only extend to the west of the Baikal Lake during the other three seasons (Figures 1a, c, and d). Especially, over the region to the north of the OS, the PMZ events during summer appear more often than those during the other three seasons. Strong persistent blockings around the OS often result in flood events over the MLRYR during summer (Sun and Zhao, 2003; Shen et al., 2008). As such, the summer higher FOPE around the OS, indicating longer-term control of blockings and ridges *in situ*, tends to play an important role in causing more precipitation over eastern China.

The climate distribution of precipitation shows that more precipitation (exceeding 160 mm) occurs over the MLRYR and its south in summer (Figure 2a). Actually, main rain belt generally appears to the south of the Yangtze River in June (Figure 2b), and then advances northwards to the MLRYR in July (Figure 2c), and finally retreats back to southern coast of China in August (Figure 2d). This is a typical monthly evolution process of the main rain belt over southern China during summer.

However, this typical evolution of rain belt may be changed due to abnormal atmospheric circulation in some specific years. For example, in 1980, the main rain belt stayed over the MLRYR for a longer time since a stronger and farther-southward western Pacific subtropical high (WPSH) during August (Zhao, 1999). As such, more August precipitation appeared over the MLRYR, which accounted for 40% of summer precipitation amount *in situ* in 1980, much higher than the climate-mean one (28%). Furthermore, this process in 1980 is not merely occasional. According to the result based on expanded empirical orthogonal function (Chen et al., 2007), this kind of process should be considered as one of most dominant modes of rain belt's evolution during summer. This signifies that, in some specific situations, precipitation in a particular month has a greater contribution to summer precipitation amount over the MLRYR. Evidently, it is worthy of exploring that the relationship between the FOPE and precipitation over eastern China during each month of summer and during the whole summer.

3.2 Precipitation and large-scale atmospheric circulation anomalies associated with the FOPE

Figure 3 presents the correlation of summer precipitation over eastern China with the simultaneous FOPE over the region between 110°E and 130°E (hereinafter called 110°–130°E FOPE) during 1979–2017. Here the latitudinal range of FOPE is not specifically confined, but the PMZ events primarily appear between 50 °N and 80°N, which can be detected in Figure 1b. Namely, all PMZ events at the mid- and high-latitudes of Eurasia are included in this analysis. As shown in Figure 3, the 110°–130°E FOPE is significantly and positively correlated with precipitation over the MLRYR region (27.5°N–33°N, 107°E–123°E). Actually, to investigate the relationship between the FOPE over different ranges of longitudes and the MLRYR precipitation, we also calculate the 5°-longitude sliding correlation coefficient between the MLRYR precipitation and the FOPE from the 30°E–50°E to 130°E–150°E regions (Figure 4a). This result further shows that, the correlation coefficient between the FOPE over the 110°E–130°E region and the MLRYR precipitation is the highest (0.56) during summer, significantly at the 99.9% confidence level (Figure 4a). In other words, the 110°E–130°E region is the most crucial region where the FOPE is closely related to the MLRYR precipitation during summer.

The correlations between the 110°E–130°E FOPE and precipitation over eastern China during June, July, and August, respectively, are displayed in Figure 5. The results further reveal that the significantly positive relationship between the 110°E–130°E FOPE and precipitation over the MLRYR region primarily exhibits during August (Figure 5c) rather than June (Figure 5a) and July (Figure 5b). Moreover, the 5°-longitude sliding correlation during August (Figure 4b) indicates that the MLRYR precipitation is also most significantly correlated with the FOPE over the 110°E–130°E region.

Figure 6 shows the time series of the August 110°E–130°E FOPE and MLRYR precipitation indices during 1979–2017. During August, the correlation coefficient between the 110°E–130°E FOPE (red line in Figure 6) and MLRYR precipitation (blue line in Figure 6) indices is up to 0.57, significant at the 99.9% confidence level.

There are 9 years (1980, 1988, 1991, 1998, 1999, 2000, 2011, 2015, and 2017) with the 110°E–130°E FOPE higher than 9 days, which indicates that the PMZ events occupied the 110°E–130°E region for approximately 30% of all 31 days in August. The 9-year mean precipitation over the MLRYR during August is 181.04 mm, considerably more than climate mean precipitation (152.26 mm) *in situ*. Moreover, the 9-year mean MLRYR precipitation in August is even more than that (170.09 mm) in July, which implies that the main rain belt commonly tends to stay and govern over the MLRYR corresponding to more PMZ events over the 110°E–130°E region during August.

There are 6 years (1985, 1986, 1997, 2003, 2012, 2016) with the 110°E–130°E FOPE lower than 2 days. That is, there was no or very less PMZ events over the 110°E–130°E region during August. The 6-year mean precipitation over the MLRYR during August is 115.79 mm, clearly less than climate mean precipitation (152.26 mm) *in situ*. The 6-year mean MLRYR precipitation in August is much less than that (182.85 mm) in July. This implies that the main rain belt generally cannot stay over the MLRYR in the absence of PMZ events over 110°E–130°E region during August.

The composite difference of precipitation between the years with the August high and low FOPE shows that, precipitation over the MLRYR does not manifests significant anomalies during July (Figure 7a), but exhibits significant positive anomalies during August (Figure 7b). This further implies that, accompanied with the higher FOPE appearing over 110°E–130°E, the main rain belt is normal during July, but still govern the MLRYR rather than withdraw back during August, therefore resulting in more precipitation over the MLRYR at that time.

In short, the aforementioned results signify that, among all PMZ events over Eurasia, those over the 110°E–130°E region seem to be of most importance in relating to the MLRYR precipitation during summer. Moreover, this close relationship primarily manifests during August, which is possibly due to that the PMZ events over the 110°E–130°E region generally tend to postpone the southward retreat of main rain belt and make it stay around the MLRYR in August. Thus, August large-scale atmospheric circulation anomalies associated with 110°E–130°E FOPE and their climate affects are further discussed.

Firstly, circulation anomalies associated with the MLRYR precipitation are shown to explain the reason for the variation of August MLRYR precipitation. During August, anomalous 500-hPa geopotential heights regressed upon the MLRYR precipitation (Figure 8a) approximately shows an East Asian/Pacific (EAP) teleconnection pattern (Huang and Sun, 1992; Lu, 2004), which is characterized by a positive geopotential height anomaly at the high-latitude area over the Stanovoy Mountains (SM) and OS region, a negative geopotential height anomaly over the mid-latitude area of East Asia, and positive geopotential height anomaly over the western Pacific subtropical area at the 500-hPa level (Bueh et al., 2008; Shi et al., 2009). This is a typical pattern contributing to precipitation over the MLRYR. Accompanying the positive geopotential height anomaly to the west of the OS, anomalous 850-hPa anticyclone appears *in situ* and induces an anomalous northeastward cold flow along the southeastern flank of this anticyclone (Figure 8b). Moreover, the positive geopotential height anomaly over the western Pacific subtropical area reflects a stronger and farther-southward WPSH. Correspondingly, anomalous 850-hPa anticyclone occurs and transports warm air to the MLRYR along the northwestern flank of this anticyclone (Figure 8b). The anomalous cold flow and warm air meet over the MLRYR and consequently facilitate more precipitation *in situ*.

The formation of the EAP pattern can be partly attributed to meridional propagation of quasi-stationary Rossby wave, which is triggered by the anomalous convective activity in the western Pacific warm pool (Nitta, 1987; Huang and Sun, 1992). Furthermore, Rossby wave packets over the high- and mid-latitude Eurasia propagate toward East Asia in upper troposphere and play an important role in forming the high- and mid-latitude anomalies of the EAP pattern (Bueh et al., 2008; Shi et al., 2009). That is, the EAP pattern is resulted from an interaction between high and lower-latitude circulation systems (Bueh et al., 2008; Shi et al., 2009). According to the latter theory (Bueh et al., 2008; Shi et al., 2009), it is highly possible that the PMZ events frequently appearing over 110°E–130°E region, which are measured by the 110°E–130°E FOPE, are responsible for, to some extent, the high- and mid-latitude height anomalies of the EAP pattern during August.

Anomalous 500-hPa geopotential heights regressed upon the 110°E–130°E FOPE

(Figure 8c) bear a similar EAP-like pattern, with a stronger and more significant positive anomaly around the SM and OS region, centered around (55°N, 130°E). This implies that, the higher (lower) 110°E–130°E FOPE can effectively represent the mid-high latitude blockings and ridges more frequently (seldom) appearing and governing over the SM and OS region during August, and accordingly dominates the month-mean anomaly of 500-hPa gepotential height *in situ*.

Corresponding to the EAP-like pattern associated with the higher 110°E–130°E FOPE (Figure 8c), anomalous 850-hPa winds over East Asian coast (Figure 8d) are also similar to those modulating the MLRYR precipitation (Figure 8b), with the anomalous cold northeasterly and warm southwesterly converging over the MLRYR region (Figure 8d) and therefore favoring more precipitation *in situ*, and vice versa.

It should be indicated that, although there is a 110°E–130°E FOPE-related positive anomaly over the western Pacific subtropical area (Figure 8c), it is hard to declare that PMZ event stimulates such an anomaly according to the present theories. However, after removing the variability of geopotential height averaged over the western Pacific subtropical area (15°N–25°N, 115°E–140°E) using the method of linear fitting (Hu et al., 2012), the individual variability of 110°E–130°E FOPE is still closely related to the high- and mid-latitude anomalies of the EAP pattern at the 500-hPa level (Figure 9a), and is therefore intimately linked with the MLRYR precipitation (Figure 9b), with a correlation coefficient of 0.42, significant at the 99% confidence level. This result further supports the notion that the development of the negative geopotential height anomaly over East Asian mid-latitude area is partly emanated from Rossby-wave energy dispersion of the positive geopotential height anomaly near the OS (Shi et al., 2009). In contrast, after removing the variability of 110°E–130°E FOPE, the individual variability of geopotential height averaged over the western Pacific subtropical area is not closely related to the MLRYR precipitation anymore (not shown), with the correlation coefficient decreasing from 0.45 to 0.23.

Certainly, in some specific years, the WPSH anomaly seems to play an more important role and disturb the relationship between the 110°E–130°E FOPE and MLRYR precipitation. For instance, although there was higher FOPE over 110°E–130°E region in August 1998, the rain belt moved northwards to the lower Yellow River valley (Figure 10a), which is due to a stronger and farther-northward WPSH (Figure 10b). As a result, there was no pronouncedly more precipitation over the MLRYR during August, floods mostly happened *in situ* during June and July in 1998, caused by two processes of the Meiyu precipitation during 12–28 June and 20–30 July, respectively (Tao et al., 1998). In August 1991, although there was also higher FOPE over the 110°E–130°E region, but there was no significant precipitation anomaly over the MLRYR (Figure 10c), which is mainly attributed to no stronger WPSH governing southern China, as indicated by negative 500-hPa geopotential height anomalies (Figure 10d).

Although the above exceptions, the variability of 110°E–130°E FOPE is undoubtedly important in modulating precipitation over the MLRYR during August. Therefore, it is also important to explore whether the August 110°E–130°E FOPE can be successfully predicted. Recently, the Next Generation Global Prediction System

(NGGPS) is used to predict PMZ events by He et al (2018). Nevertheless, their results show that the skill score associated with the FOPE is generally lower in the Euro-Atlantic-Asia sector than in the Pacific-North America sector. To provide an additional tool or guidance to predict the FOPE in a specific region of Asia (i.e., 110°E–130°E), we further explore preceding atmospheric signals through statistical analyses, which may also help to improve the prediction of the MLRYR precipitation.

4. Preceding atmospheric signals of the 110°E–130°E FOPE

The correlation between the August 110°E–130°E FOPE and previous July 500-hPa geopotential heights during 1979–2017 (Figure 11) shows that there are three significantly positive correlations near the SM, the Balkhash Lake (BL), and the Caucasus region (CR), respectively. The preceding signals of significant correlations generally appear over the SM region and its west at the mid- and high-latitudes, implying that the August 110°E–130°E FOPE can possibly be tracked to upstream atmospheric circulation anomalies during previous July. The correlation analysis further reveals that no significant correlations can be detected at the mid-high latitudes during the earlier month (i.e., June; not shown). The results imply that the July mid-high-latitude atmospheric circulation anomalies are probably applied in statistically predicting the August 110°E–130°E FOPE, but the earlier (June) ones are not.

Based on Figure 11, the regionally averaged 500-hPa geopotential height over the SM (52°–60°N, 126°–140°E; the box on the right), BL (39°–46°N, 72°–90°E; the box in the middle), and CR (36°–46°N, 30°–50°E; the box on the left) is defined as the

SM, BL, and CR height indices, respectively. Using the three indices, the effects of the July geopotential height anomalies over the three key regions on the 110°E–130°E FOPE during the ensuing August are further investigated.

The correlation coefficient between the July SM height index and the August 110°E–130°E FOPE is 0.35, significant at the 95% confidence level. However, the correlation between the July SM height index and the ensuing August 500-hPa geopotential heights displays a significantly positive correlation to the east of Japan (not shown), where is farther east relative to the FOPE-related region where a center of significantly positive correlation appears (Figure 8c). This implies that the July geopotential height anomaly over the SM seems to affect its eastern (downstream) geopotential height anomaly rather than local one during the next month. Therefore, the July SM height index should not be regarded as a signal that is directly related to the August 110°E–130°E FOPE. It is possible that one or multiple factors affect both the July geopotential height anomaly over the SM and the August 110°E–130°E FOPE, and consequently result in their indirect link. However, it might be a complicated physical process and would not be discussed in the present paper.

The correlation coefficient between the July BL height index and the August 110°E–130°E FOPE is 0.39, significant at the 95% confidence level. The correlation between the July BL height index and simultaneous 500-hPa geopotential heights (Figure 12a) shows that a significantly positive correlation extends northeastwards from the BL region to the region around the Baikal Lake. During August, the significantly positive correlation continues to extend northeastwards and eventually forms a center around the SM and OS region (Figure 12b). The results imply that the geopotential height anomaly over the BL region may relay its impact through extending northeastwards during July–August. A potential process is speculated as follows. High-pressure systems appear over the BL region during July, and then they gradually move northeastwards during July–August and eventually develop and form PMZ events around 110°E–130°E and result in month-mean geopotential height anomalies over the FOPE-related region (i.e., the SM and OS region; Figure 12b) during August. It should be pointed out that the high-pressure systems over the BL may not reach the threshold of PMZ event's strength during July. However, with their continuous moving and developing from July until August, the high-pressure systems act to facilitate the formation of PMZ events and make them frequently appear around 110°E–130°E. As such, the July BL height index is closely related with the 110°E–130°E FOPE and with month-mean geopotential height anomaly over the SM and OS region during August (Figure 12b).

The correlation coefficient between the July CR height index and the August 110°E–130°E FOPE is 0.41, significant at the 99% confidence level. Figure 13a displays that, apart from a local high correlation, the geopotential height anomaly over the CR is also remotely correlated with that over the BL, forming a positive-negative-positive pattern from the CR to the BL during July. Similarly, the BL height anomaly continually extends northeastwards and notably modulates the 110°E–130°E FOPE and associated geopotential height anomaly during July–August (Figure 13).

In effect, the geopotential height anomaly over the CR is closely connected with that over the BL region during July, with a correlation coefficient of 0.56 (significant at the 99.9% confidence level), and the latter can relay its effect through extending northeastwards during July–August. Therefore, it is necessary to further understand whether the variation of the July BL height index itself is sufficient to adjust the 110°E–130°E FOPE or the variation of the July CR height also play a crucial role in this process. To examine the individual effect of the BL height anomaly when the variability of the July CR height index is absent, an individual BL height index is obtained through removing the CR height index-related variation. Figure 14a presents the correlation between the individual BL height index and 500-hPa geopotential heights during July, which reveals that the individual geopotential height anomaly over the BL region is confined to a local area rather than extends northeastwards, which causes a non-significant correlation (only 0.19) between the individual July BL height index and the August 110°E–130°E FOPE. The result indicates that the July BL height anomaly itself is not enough to effectively affect the August 110°E–130°E FOPE. Meanwhile, this result also implies that the variation of the July CR geopotential height can also contribute to that of the August 110°E–130°E FOPE, and therefore the former should also be considered as an important signal for the latter.

To further emphasize the synthesized effect of the BL and CR height anomalies, a new BL-CR height index is calculated by a simple arithmetic mean of the BL and CR height indices. The correlations of July (Figure 14b) and August (Figure 14c) 500-hPa geopotential heights with the July BL-CR height index clearly shows a relay-like northeastward extension from the BL to the SM and OS region via the Baikal Lake. This further reveals that, after superimposing the effect of the CR height anomaly, the synthesized effect of the July BL and CR height anomalies considerably boosts this northeastward extension of geopotential height anomaly during July–August relative to the individual effect of the July BL height anomaly (Figure 14a). As a result, the July BL-CR height index is closely related to the August 110°E–130°E FOPE, with a correlation coefficient of 0.46, significant at the 99% confidence level, which is higher than the correlation coefficients of the August 110°E–130°E FOPE with the July BL (0.39) and CR (0.41) height indices, respectively.

In addition, the 200-hPa geopotential heights related to the synthesized variation of the CR and BL height anomalies during July show a clear wave-train pattern from the tropical Atlantic to East Asia and it adjacent Pacific (Figure 15a). Moreover, the northeastward extension from the BL to the Baikal Lake is also clear at the upper-tropospheric level, which further indicates that the preceding atmospheric signal of the August 110°E–130°E FOPE is closely related to the upper-tropospheric wave-train pattern. The 200-hPa ***v***-winds related to the synthesized variation of the CR and BL height anomalies during July (Figure 15b) evidently show a Silk Road Pattern (SRP; Lu et al., 2002; Sato and Takahashi, 2006; Yasui and Watanabe, 2010; Chen and Huang, 2012; Hong et al., 2018). Apparently, it is worthy of further investigation that the relationship between the preceding July SRP and anomalous activities of PMZ events over the 110°E–130°E region during August and associated physical mechanism in the future.

5. Summary and discussion

Based on an updated approach developed by Liu et al. (2017), which can effectively identify and track persistent ridges and blockings as PMZ events, a FOPE is defined to reflect time length when and domain where PMZ events govern during some period. The relationships between the FOPE over different regions of Eurasia and precipitation over eastern China are explored. The results shows that, among PMZ events occurring over Eurasia, those over the 110°E–130°E region have the closest relationship with the MLRYR precipitation during summertime, in particular, during August. This may, to some extent, be attributable to that the PMZ events over the 110°E–130°E region generally tend to postpone the southward retreat of main rain belt and make it reside around the MLRYR in August.

The 110°E–130°E FOPE can effectively reflect more frequently (seldom) activities of the blockings and ridges near the OS, and therefore is also linked with the month-mean anomaly of 500-hPa gepotential height *in situ* during August. Through southward Rossby-wave energy dispersion of the geopotential height anomaly near the OS (Shi et al., 2009), the 110°E–130°E FOPE is closely related to the high- and mid-latitude anomalies of the EAP pattern. Together with the low-latitude anomaly of the EAP pattern, the high- and mid-latitude anomalies of the EAP pattern associated with the 110°E–130°E FOPE induce a convergence of cold and warm flows over the MLRYR, and hence modulate precipitation *in situ*.

Moreover, the preceding atmospheric signals of the August 110°E–130°E FOPE are studied. The July geopotential height anomaly over the BL region can extend northeastwards from the BL to SM and OS regions during July–August. This relay-like northeastward extension implies the following potential process, that is, high-pressure systems appear over the BL region (although they may not reach the strength level of PMZ events) during July and then gradually move northeastwards during July–August and finally develop and facilitate the occurrence of PMZ events around 110°E–130°E during August. The geopotential height anomaly over the CR is closely linked with the one over the BL through a positive-negative-positive wave train during July, and therefore also contributes to the variation of the August 110°E–130°E FOPE. Further analyses suggest that the synthesized effect of the July CR and BL height anomalies can pronouncedly intensify the northeastward extension of geopotential height anomaly during July–August. Therefore, to reflect the synthesized variation of the July CR and BL height anomalies, a BL-CR height index is defined and is found to be significantly correlated with the August 110°E–130°E FOPE. Relative to the BL and CR height indices, the July BL-CR height index gives a better performance in predicting the August 110°E–130°E FOPE, and therefore should be considered as one of the important predictors. The CR and BL height anomalies are directly linked with the SRP during July. It should be further discussed how and why the preceding July SRP can indicate the August 110°E–130°E FOPE in the future.

It is also noted that, although the July BL-CR height index is closely related to the August 110°E–130°E FOPE, but it is not significantly correlated with August geopotential heights over the western Pacific subtropical area (i.e., the low-latitude anomaly center of the EAP pattern), with a low correlation coefficient of 0.13. The result indicates that the July BL-CR height index cannot successfully predict the low-latitude component of the EAP pattern. Despite that, the correlation coefficient between the July BL-CR height index and August the MLRYR precipitation is 0.27 during 1979–2017, still at the 90% confidence level. In the future, we should further explore new predictors for August geopotential height over the western Pacific subtropical area, which should also be combined with the preceding July BL-CR height index to predict the entire anomalous structure of the EAP pattern. This combination of multiple predictors may have a higher skill in predicting related MLRYR precipitation during August.

Acknowledgments

This work was jointly sponsored by the Support Plan of the National Science and Technology (2015BAC03B04), the National Key Research and Development Program of China (Grant 2018YFC1505706), the Strategic Priority Research Program of Chinese Academy of Sciences (Grant XDA20100300), the National Science Foundation of China (Grants 41375090 and 91637312), and the Research Fund of the Chinese Academy of Meteorological Sciences (Grants 2019KJ022 and 2017Z013).

References

Bi M, Ding Y. 1992. A study of budget of potential vorticity of blocking high during the drought period in summer of 1980. *Quart. J. Appl. Meteor. (in Chinese)* **3:** 145–156.

Black E, Blackburn M, Harrison G, Hoskins B, Methven J. 2004. Factors contributing to the summer 2003 European heatwave. *Weather* **17:** 4080–4088.

Bueh C, Shi N, Ji L, Wei J, Tao S. 2008. Features of the EAP events on the medium-range evolution process and the mid- and high-latitude Rossby wave activities during the Meiyu period. *Chinese Sci. Bull.* **53:** 610–623.

Bueh C, Xie Z. 2015. An objective technique for detecting large-scale tilted ridges and troughs and its application to an East Asian cold event. *Mon. Wea. Rev.* **143:** 4765–4783.

Buehler T, Raible CC, Stocker TF. 2011. The relationship of winter season North Atlantic blocking frequencies to extreme cold or dry spells in the ERA-40. *Tellus A* **63:** 212–222.

Cattiaux J, Vautard R, Cassou C, Yiou P, Masson-Delmotte V, Codron F. 2010. Winter 2010 in Europe: A cold extreme in a warming climate. *Geophys. Res. Lett.* **37:** L20704, doi:10.1029/2010GL044613.

Chen G, Huang R. 2012. Excitation mechanisms of the teleconnection patterns affecting the July precipitation in Northwest China. *J. Clim.* **25:** 7834–7851.

Chen L, Zong H, Zhang Q. 2007. The dominant modes of intraseasonal variability of summer monsoon rain belt over eastern China. *Chinese J Atmos. Sci.* (in Chinese) **31:** 1212–1222.

Dole RM, Hoerling M, Perlwitz J, Eischeid J, Pegion P, Zhang T, Quan XW, Xu T, Murray D. 2011. Was there a basis for anticipating the 2010 Russian heat wave? *Geophys. Res. Lett.* **38:** L06702, doi:10.1029/2010GL046582.

Green J. 1977. The weather during July 1976: Some dynamical considerations of the drought. *Weather* **32:** 120–126.

Gu W, Chen L, Zuo J, Li W. 2016. Combined effect of multiple factors on the summer rainfall anomalies over the Huanghe-Huaihe valley in 1992 and 1998. *Chinese J. Atmos. Sci. (in Chinese)* **40:** 743–755.

He B, Liu P, Zhu Y, Hu W. 2018. Prediction and predictability of Northern Hemisphere persistent maxima of 500-hPa geopotential height eddies in the GEFS. *Clim. Dyn.* doi: 10.1007/s00382-018-434-4.

Hong X, Lu R, Li S. 2018. Asymmetric relationship between the meridional displacement of the Asian Westerly Jet and the Silk Road Pattern. *Adv. Atmos. Sci.* **35:** 389–396.

Horton RM, Mankin JS, Lesk C, Coffel E, Raymond C. 2016. A review of recent advances in research on extreme heat events. *Curr. Clim. Change Rep.* **2:** 242–259.

Hoskins BJ, Woollings T. 2015. Persistent extratropical regimes and climate extremes. *Curr. Clim. Change Rep.* **1:** 115–124.

Hu M, Gong D, Wang L, Zhou T, Zhang Z. 2012. Possible influence of January-March Arctic Oscillation on the convection of tropical North Pacific and North Atlantic (in Chinese). *Acta Meteorol. Sin.* **70:** 479–491.

Huang R, Sun F. 1992. Impact of tropical western Pacific on the East Asian summer monsoon. *J. Meteor. Soc. Japan* **70:** 243–256.

Kaas E, Branstator G. 1993. The relationship between a zonal index and blocking activity. *J. Atmos. Sci.* **50:** 3061–3077.

Kalnay E, and Coauthors. 1996. The NCEP/NCAR 40-Year Reanalysis Project. Bull. Amer. *Meteor. Soc.* **77:** 437–471.

Liu P, Zhu Y, Zhang Q, Gottschalck J, Zhang M, Melhauser C, Li W, Guan H, Zhou X, Hou D, Peña M, Wu G, Liu Y, Zhou L, He B, Hu W, Sukhdeo R. 2018. Climatology of tracked persistent maxima of 500-hPa geopotential height. Clim. Dyn. **51:** 701–717.

Lu R, Huang R. 1999. Influence of the stationary disturbance in the Westerlies on the blocking highs over the Northeastern Asia in summer. Chinese *J. Atmos. Sci. (in Chinese)* **23:** 533–542.

Lu R, Oh JH, Kim BJ. 2002. A teleconnection pattern in upper-level meridional wind over the North African and Eurasian continent in summer. *Tellus A* **54:** 44–55.

Lu R. 2004. Associations among the components of the East Asian summer monsoon system in the meridional direction. *J. Meteor. Soc. Japan* **82:** 155–165.

Lukas B, Gabriele C, Andrea K. 2017. Connecting atmospheric blocking to European temperature extremes in Spring. *J. Clim.* **30:** 585–594.

Matsueda M. 2011. Predictability of Euro-Russian blocking in summer of 2010. *Geophys. Res. Lett.* **38:** L06801, doi:10.1029/2010GL046557.

Nitta T. 1987. Convective activities in the tropical western Pacific and their impact on the Northern Hemisphere summer circulation. *J . Meteor. Soc. Japan* **65:** 373–390.

Parsons S, Renwick J, McDonald A. 2016. An assessment of future Southern

Hemisphere blocking using CMIP5 projections from four GCMs. *J. Clim.* **29:** 7599–7611.

Pfahl S, Wernli H. 2012. Quantifying the relevance of atmospheric blocking for co-located temperature extremes in the Northern Hemisphere on (sub-) daily time scales. *Geophys. Res. Lett.* **39:** L12807, doi:10.1029/2012GL052261.

Renwick J. 2005. Persistent positive anomalies in the Southern Hemisphere circulation. *Mon. Weather Rev.* **133:** 977–988.

Sato N, Takahashi M. 2006. Dynamical processes related to the appearance of quasi-stationary waves on the subtropical jet in the midsummer northern hemisphere. *J. Clim.* **19:** 1531–1544.

Shen A, Ren G, Wang B. 2008. Analysis and forecasting of relationship between East-Asia Blocking situation and precipitation of China in July. *Clim. Environ. Res. (in Chinese)* **13:** 206–211.

Shi N, Bueh C, Ji L, Wang P. 2009. Impacts of mid- and high-latitude Rossby wave activities on the medium-range evolution of East Asia/Pacific events during the mid- and late summer. *Chinese J. Atmos. Sci.* (in Chinese), **33:** 1087–1100.

Sun J, Zhao S. 2003. A study of special circulation during Meiyu season of the Yangtze River basin in 1998. *Clim. Environ. Res. (in Chinese)* **8:** 291–306.

Tao S, Zhang Q, Zhang S. 1998. The great floods in Changjiang River valley in 1998. *Clim. Environ. Res.* (in Chinese) **3:** 290–299.

Wu G, Liu H, Chen F, Zhao Y. 1994. Transient eddy transfer and formation of blocking high on the persistently abnormal weather in the summer of 1980. *Acta*

Meteor. Sin. (in Chinese) **52:** 308–320.

Xie P, Arkin PA. 1997. Global precipitation: A 17-year monthly analysis based on gauge observations, satellite estimates, and numerical model outputs. *Bull. Amer. Meteor. Soc.* **78:** 2539–2558.

Yasui S, Watanabe M. 2010. Forcing processes of the summertime circumglobal teleconnection pattern in a dry AGCM. *J. Clim.* **23:** 2093–2114.

Ye P, Li Y, Wang S, Wang Y, Shang K. 2015. Variation characteristics of different atmospheric blockings and their impact on temperature over the Northern Hemisphere. *J Lanzhou University (Nat. Sci.)* **51:** 639–645.

Yin H, Li C. 2001. Human impact on floods and flood disasters on the Yangtze River. *Geomorphology* **41:** 105–109.

Yu S, Lin X. 2006. Characteristics of two general circulation patterns during floods over the Changjiang Huaihe River Valley. *Acta Meteor. Sin. (in Chinese)* **64:** 605–613.

Zhang Q, Tao S. 1998. Influence of Asian mid-high latitude circulation on East Asian summer rainfall. *Acta Meteor. Sin. (in Chinese)* **56:** 199–211.

Zhang Q, Xu C, Zhang Z, Chen YD, Liu C, Lin H. 2008. Spatial and temporal variability of precipitation maxima during 1960–2005 in the Yangtze River basin and possible association with large-scale circulation. *J. Hydrol.* **353:** 215–227.

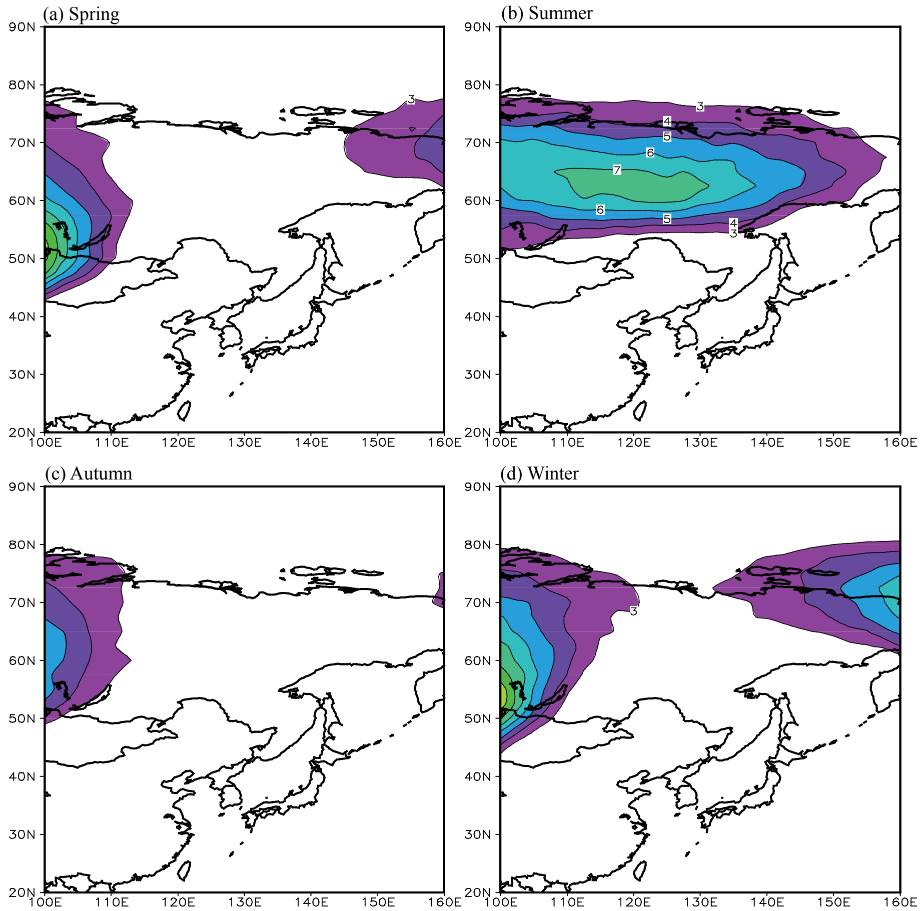

Figure 1. Climate mean distribution of the (a) spring, (b) summer, (c) autumn, and (d) winter FOPE during 1979–2017

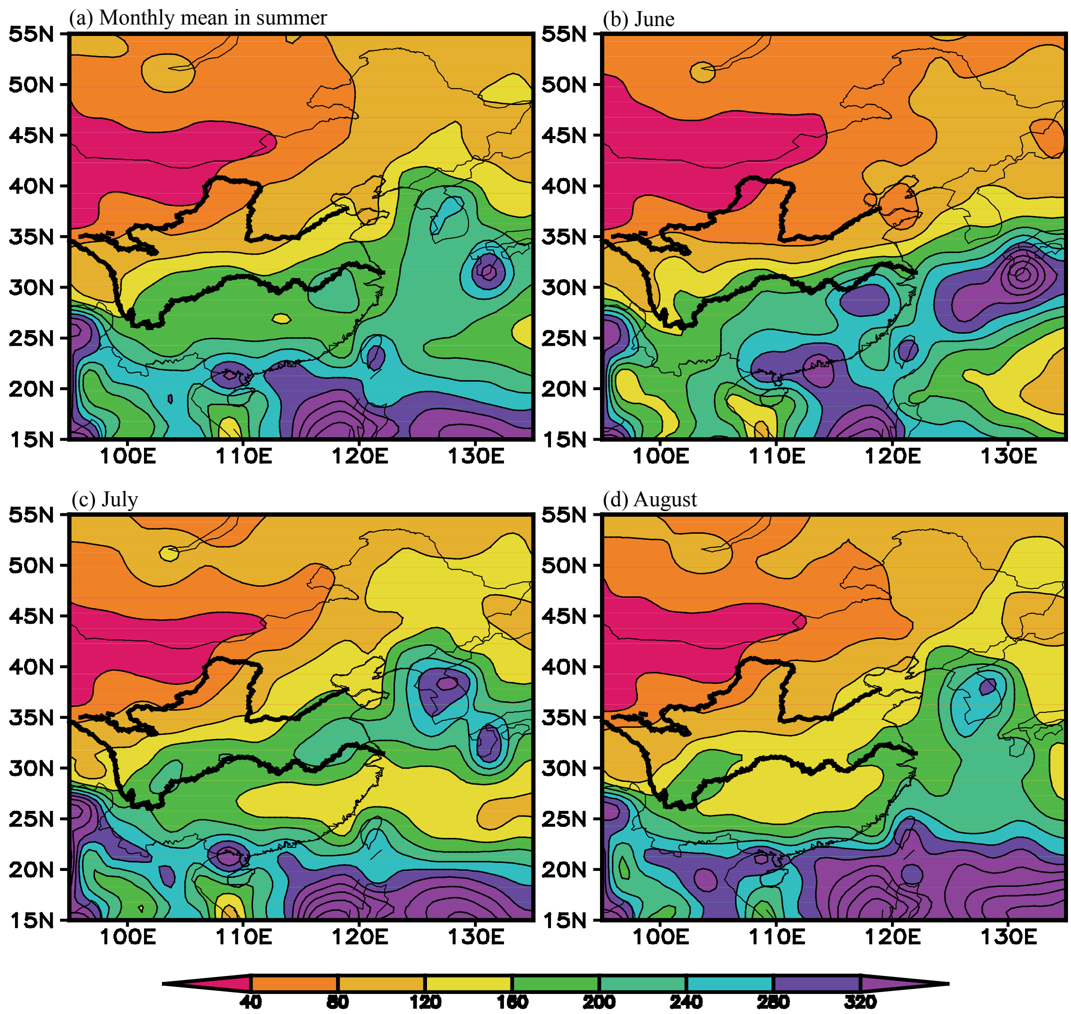

Figure 2. Climate mean distribution of (a) summer monthly mean, (b) June, (c) July, and (d) August precipitation (units: mm) over eastern China during 1979–2017. The amount of summer precipitation is the value of monthly mean precipitation multiplied by 3. The upper and lower thick black lines represent the Yellow and Yangtze River, respectively.

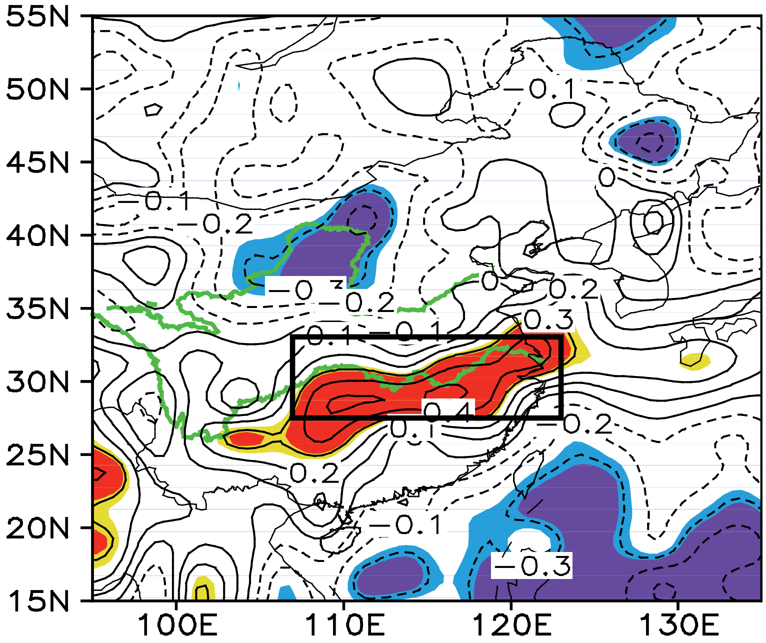

Figure 3. Distribution of correlation coefficients the summer 110°E–130°E FOPE and simultaneous precipitation over eastern China during 1979–2017. Yellow (red) shading denotes positive correlations significant at the 90% (95%) confidence level. The black box represent the MLRYR region (27.5°N–33°N, 107°E–123°E). The upper and lower thick green lines represent the Yellow and Yangtze River, respectively.

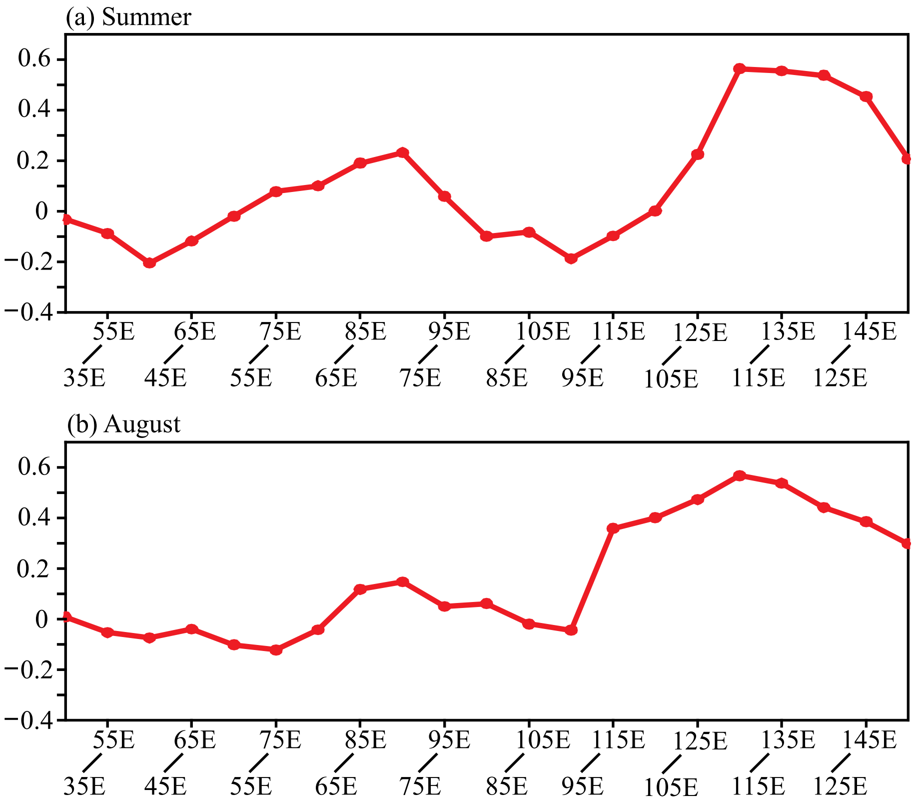

Figure 4. 5°-longitude sliding correlation coefficient between the MLRYR precipitation and the FOPE from the 30°E–50°E to 130°E–150°E regions during (a) summer and (b) August for the period of 1979–2017.

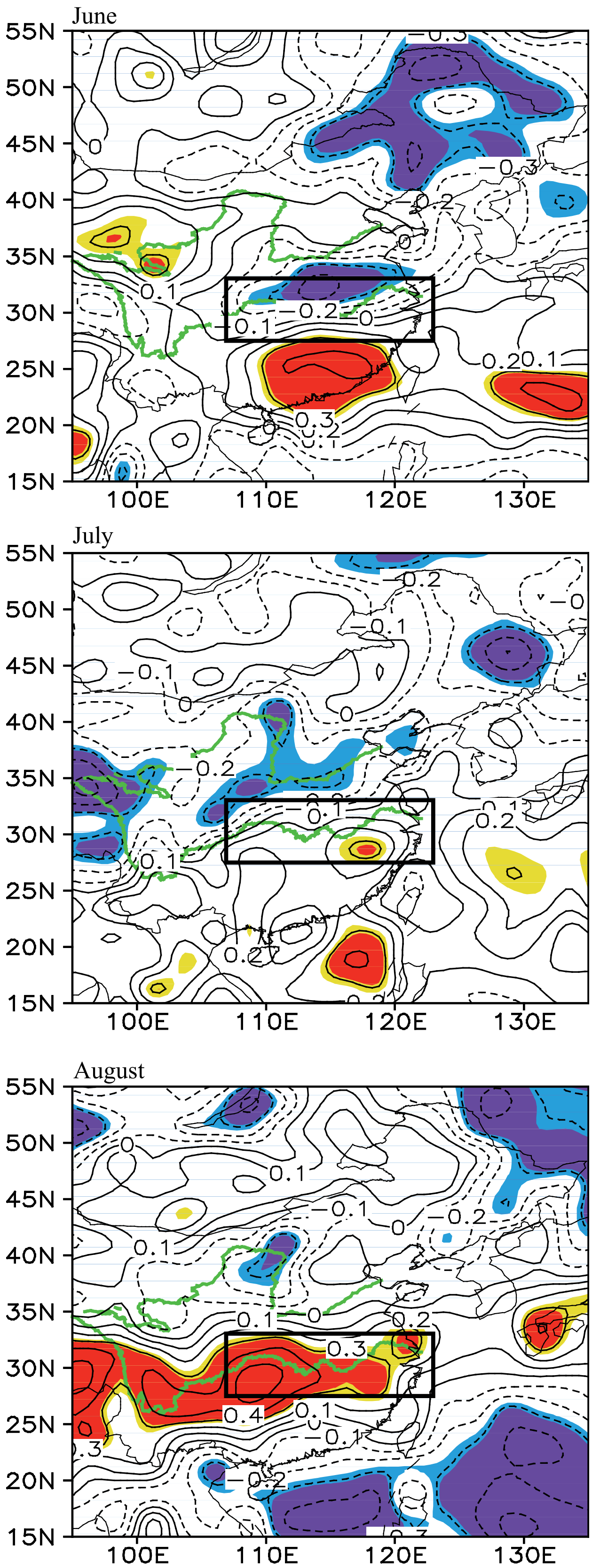

Figure 5. As in Figure 3, but for June, July, and August, respectively.

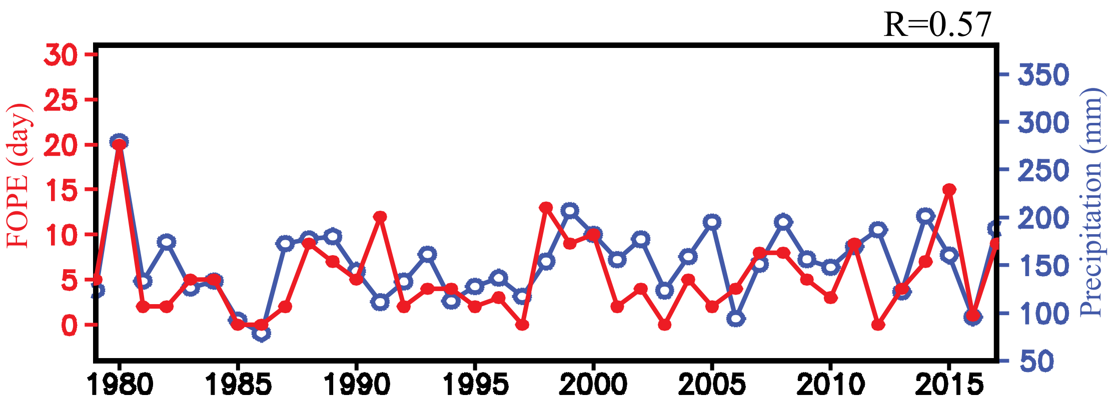

Figure 6. Time series of the August the 110°E–130°E FOPE (red line; units: days) and simultaneous MLRYR precipitation (blue line; units: mm) indices during 1979–2017. The correlation coefficient between the two indices is 0.57, significant at the 99.9% confidence level.

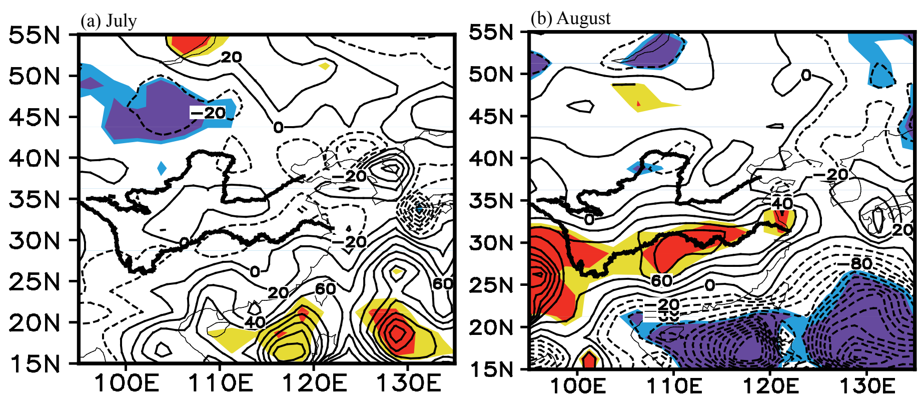

Figure 7. Composite difference of (a) July and (b) August precipitation between the years with the August high and low FOPE (high minus low). Yellow (red) shading denotes positive precipitation anomalies significant at the 90% (95%) confidence level, and blue (purple) shading indicates negative precipitation anomalies significant at the 90% (95%) confidence level.

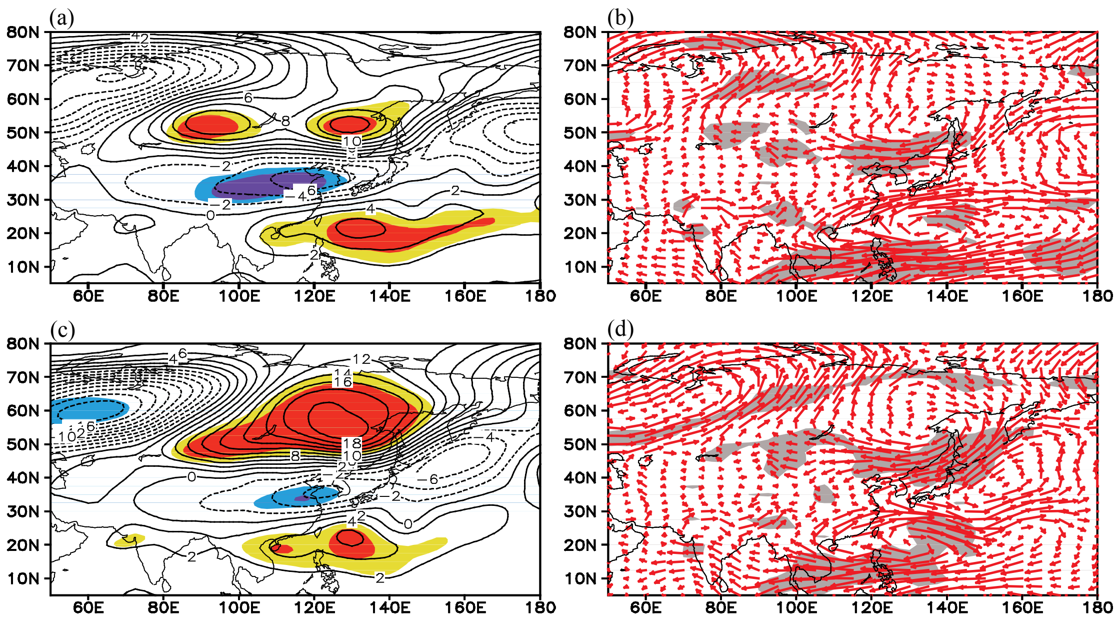

Figure 8. Anomalous August (a) 500-hPa geopotential height (units: gpm) and (b) 850-hPa winds (units: m/s) regressed upon the simultaneous MLRYR precipitation index for the period 1979–2017. (c, d) As in (a, b), respectively, but for the regression upon the 110°E–130°E FOPE.

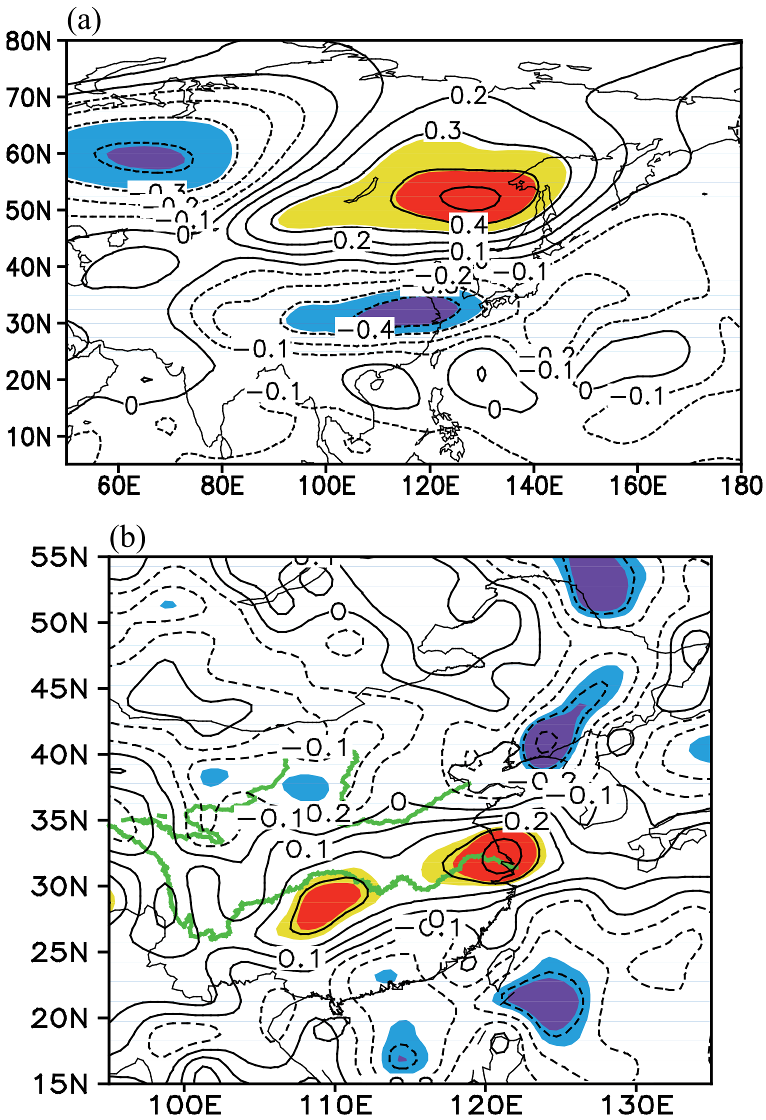

Figure 9. Distribution of the correlation coefficients of (a) 500-hPa geopotential heights and (b) precipitation with the individual 110°E–130°E FOPE index after removing the variability of geopotential heights averaged over the western Pacific subtropical area during August for the period 1979–2017. For geopotential heights (a), yellow (red) shading denotes positive correlations significant at the 95% (99%) confidence level, and blue (purple) shading indicates negative correlations significant at the 95% (99%) confidence level. For precipitation (b), the shadings also denote significance of correlation, but at the 90% (95%) confidence level.

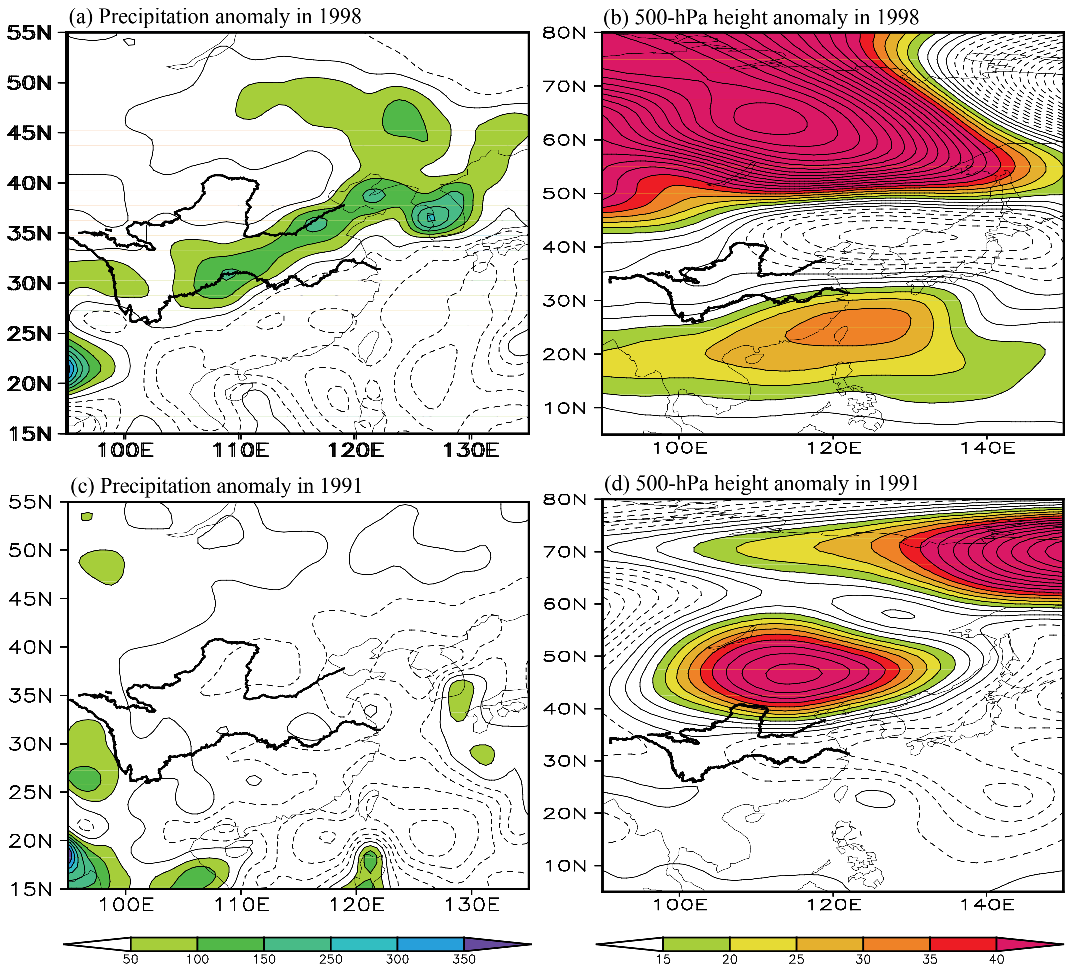

Figure 10. Anomalous August (a) precipitation (units: mm) and 500-hPa geopotential height (units: gpm) in 1998; (c) and (d) as shown in (a) and (b), but in 1991.

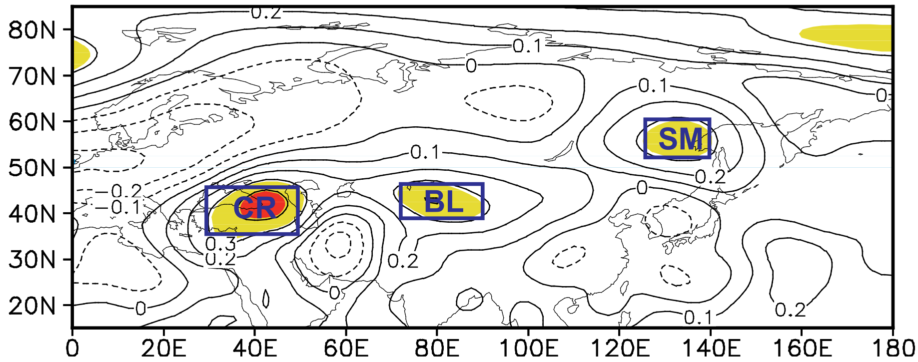

Figure 11. Distribution of correlation coefficients the August 110°E–130°E FOPE and previous July 500-hPa geopotential heights during 1979–2017. Yellow (red) shading denotes positive correlations significant at the 95% (99%) confidence level. The three blue boxes from right to left represent the SM, BL, and CR region, respectively.

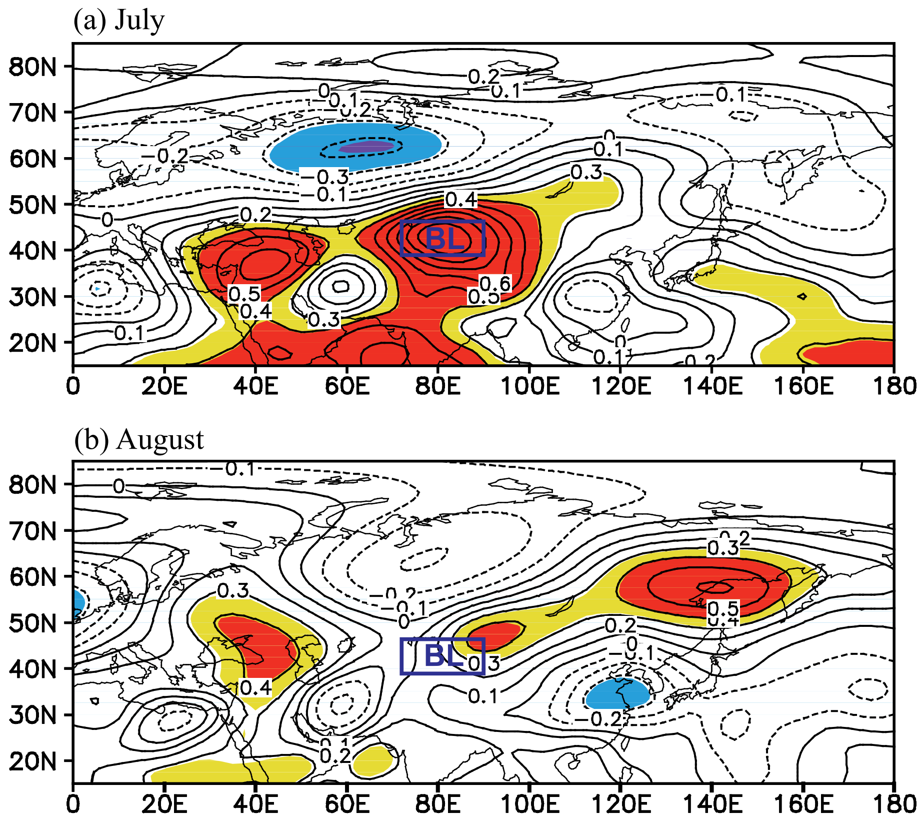

Figure 12. (a) Distribution of correlation coefficients between the July BL height index and simultaneous 500-hPa geopotential heights during 1979–2017. (b) As in (a), but for 500-hPa geopotential heights during August. Yellow (red) shading denotes positive correlations significant at the 95% (99%) confidence level, and blue (purple) shading denotes negative correlations significant at the 95% (99%) confidence level. The blue rectangle represents the BL region.

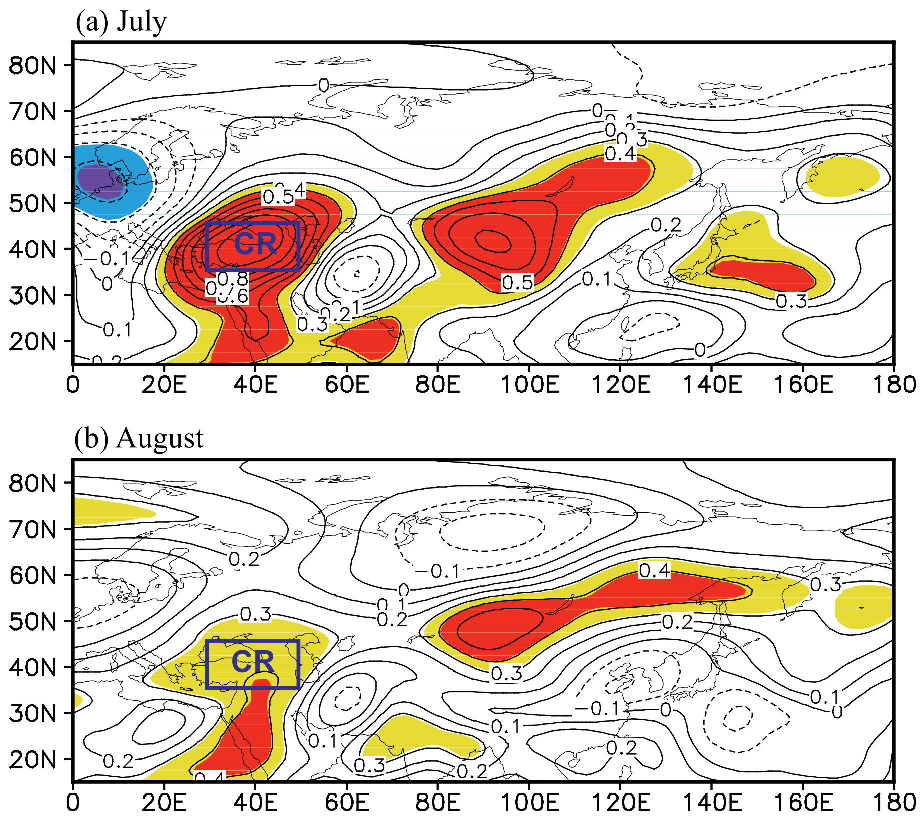

Figure 13. As in Figure 12, but for the correlations between the July CR height index and 500-hPa geopotential heights.

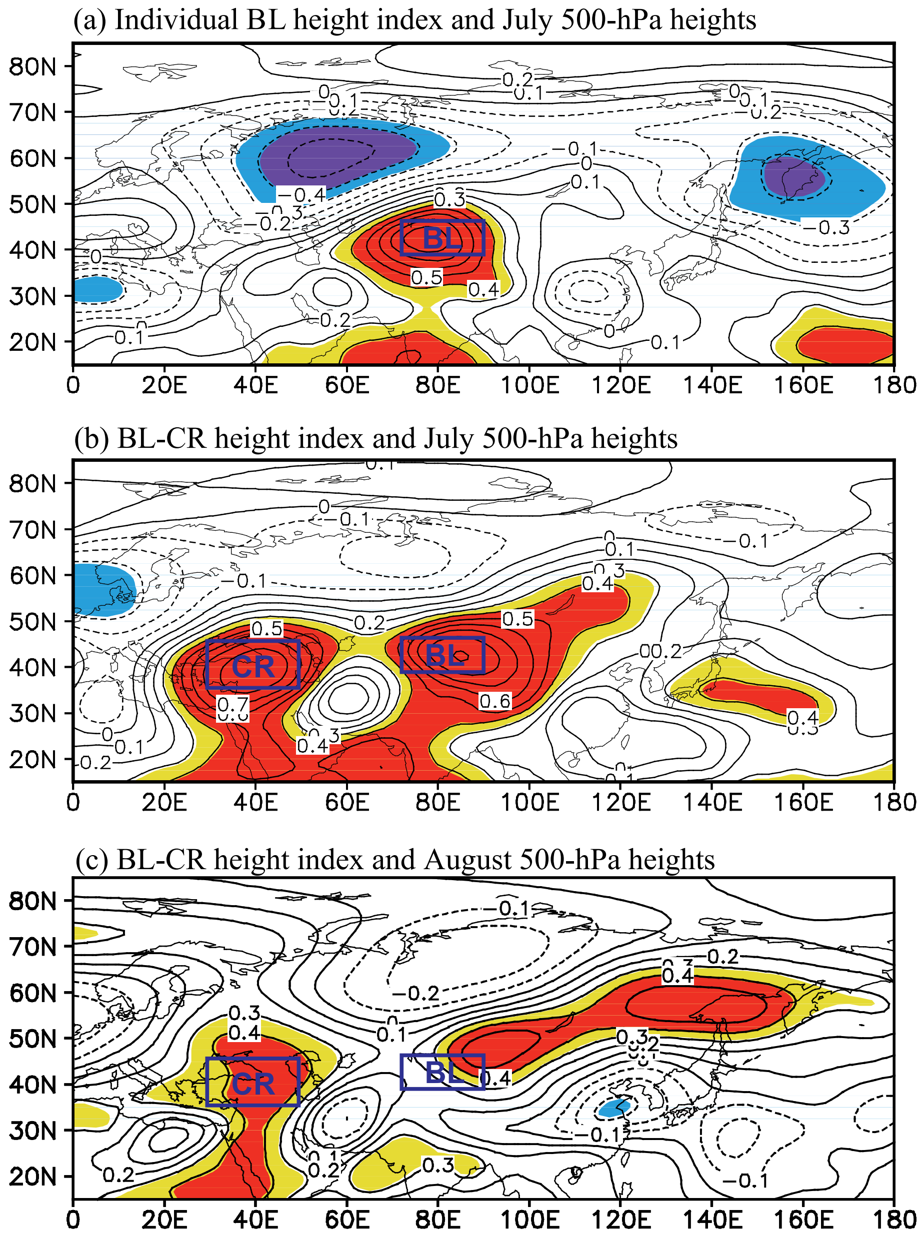

Figure 14. (a) Correlation of July 500-hPa geopotential heights with the July individual BL height index after removing the variation of the CR height index during 1979–2017. (b) As in (a), but for the correlation with the July BL-CR height index. (c) As in (b), but for the correlation of August 500-hPa geopotential heights. Yellow (red) shading denotes positive correlations significant at the 95% (99%) confidence level, and blue (purple) shading indicates negative correlations significant at the 95% (99%) confidence level.

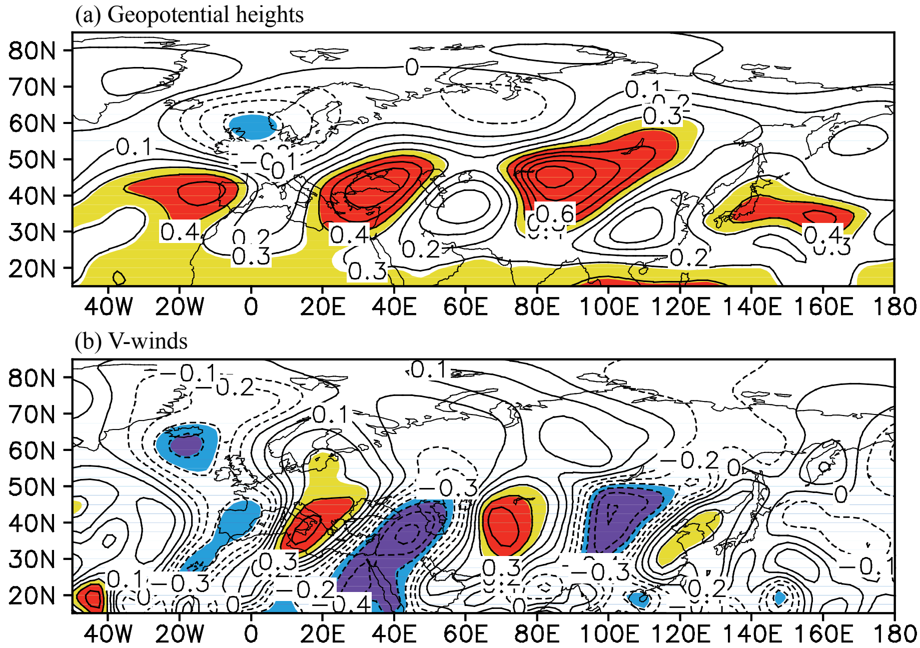

Figure 15. (a) Distribution of correlation coefficients of July 200-hPa (a) geopotential heights and (b) ***v***-winds with the simultaneous BL-CR height index during 1979–2017. Yellow (red) shading denotes positive correlations significant at the 95% (99%) confidence level, and blue (purple) shading indicates negative correlations significant at the 95% (99%) confidence level.